RP Current Trends in Engineering and Technology
Vol. 1, No. 6 (December 2022) pp. 128–136
e-ISSN: 2583-5491

RESEARCH PLATEAU PUBLISHERS

Cite this article: J. Gahlawat, Coupled mode theory of single-resonant parametric oscillation in semiconductor magneto-plasmas, *RP Cur. Tr. Eng. Tech.* **1** (2022) 128–136.

Original Research Article

Coupled mode theory of single-resonant parametric oscillation in semiconductor magneto-plasmas

Jyoti Gahlawat
Department of Physics, Baba Mastnath University, Asthal Bohar, Rohtak – 124021, Haryana, India
*Corresponding author, E-mail: jgahlawat.bmu@gmail.com

ARTICLE HISTORY
Received: 22 Oct. 2022
Revised: 28 Dec. 2022
Accepted: 29 Dec. 2022
Published online: 30 Dec. 2022

KEYWORDS
Nonlinear optics; optical parametric oscillation; coupled mode theory; semiconductor magneto-plasmas.

ABSTRACT
We have conducted an analytical investigation of the parametric oscillation of optical phonons in magnetised doped Semiconductor magneto-plasmas using the hydrodynamic model of semiconductor plasmas and coupled mode theory of interacting waves. The complicated effective second-order optical susceptibility resulting from nonlinear polarisation produced by induced current density and by interaction of the pump wave with molecular vibrations generated inside the medium is thought to be the source of nonlinear interaction. For the single resonant parametric oscillator that has been proposed, expressions have been found for the threshold pump intensity and conversion efficiency. Numerical analysis has been made for a representative n-InSb crystal irradiated by 10.6 μm pulsed CO_2 laser. On the threshold pump intensity and conversion efficiency of the single resonant parametric oscillator, the effects of some significant parameters, including the transverse magnetostatic field, mirror reflectivity, and crystal length, have been thoroughly examined. Transversely magnetised doped Semiconductor magneto-plasmas have a technological promise as hosts for parametric devices such parametric oscillators, according to the investigation.

1. Introduction

A subfield of optics called nonlinear optics studies how light behaves in nonlinear media. It deals with how electromagnetic fields that have been applied to different materials interact to create new electromagnetic fields that have different phase, frequency, amplitude, or other physical features [1-3]. Due to its widespread use in laser technology, optical communication, and data storage technology, the topic of nonlinear optics is receiving more and more attention [4, 5]. Understanding the principles of numerous nonlinear interactions is crucial for the design and functioning of a variety of prospective light-based technologies. The essential interaction among these is parametric interaction. The origin of this interaction lies in second-order optical susceptibility $\chi^{(2)}$ of the medium. In this method, a powerful laser beam—referred to as the "pump"—interacts with a nonlinear medium to produce waves with new frequencies. This happens as a result of waves being mixed together or deliberately split apart. Depending on the material's qualities and the geometry of externally applied magnetic and electric fields, the waves may then be amplified or attenuated. Successful applications of parametric interactions include the research of photon amplifiers [6] and the production of high peak power sub-picosecond optical pulses [7].

Due to its potential uses, devices based on parametric interactions, such as optical parametric amplifiers and oscillators, hold a unique place in nonlinear optics [8]. They have been widely employed in the construction of tunable coherent radiation sources with excellent gain and conversion efficiencies [9]. Over a wide frequency range, optical parametric oscillators are employed to produce coherent light and mode-locked pulse trains, typically in bands where tunable laser sources are limited [10, 11].

An optical parametric oscillator (OPO) is a device based on optical parametric oscillation which oscillates at optical frequencies. It converts an input pump wave at frequency ω_0 into two output waves of lower frequency (ω_s, ω_i) by means of second order nonlinear optical interaction. The sum of the output waves frequencies is equal to the input wave frequency: $\omega_s + \omega_i = \omega_0$. For historic reasons, the two output waves are called "signal" and "idler", where the wave with higher frequency is called signal. A special case is the degenerate OPO, when the output frequency is one-half the pump frequency, $\omega_s = \omega_i = \omega_0/2$ The main application of an OPO is to generate longer wavelengths, like pulsed lasers at around 1.55 μm, from a 1.064 μm pump. The former wavelength lies in the eye-safe band and is commonly used by range-finding devices. But an OPO can also be used to generate longer wavelengths, or various wavelengths in the visible regime when pumped at 355 nm [12].

Recent studies on gain width and rise duration of pulsed unstable OPOs as well as limited output coupling of the resonant wave have significantly improved the overall performance of continuous wave single resonant parametric oscillators (SRPOs) [13, 14]. On the basis of OPO features, numerous efficient techniques of producing eye-safe radiations and light in the yellow and blue spectral range are also being developed [15-17]. Due to the intrinsic material restrictions, such as the low optical damage threshold, insufficient

birefringence, and inadequate optical transparency range, developments in the field of OPO and their application are severely constrained.

New opportunities for producing extensively tunable optical coherent radiation with OPO have opened up with the development of new nonlinear materials with high optical damage thresholds, large optical transparency ranges, and laser pump sources with increased spectral and spatial coherence. When compared to other nonlinear materials, semiconductor crystals, especially Semiconductor magneto-plasmas, are largely transparent at photon energies much lower than band-gap energies and are susceptible to optical damage at excitation intensities that are significantly higher than average [18, 19]. In terms of compactness, control over material relaxation times, observed substantial nonlinearities in optical characteristics under near resonant laser irradiation, and advanced fabrication technology, semiconductors also have an edge over other materials [20, 21]. Additionally, these crystals contain several optically excited coherent collective modes (such as acoustical phonon mode, optical phonon mode, polaron mode, polariton mode etc.) Additionally, a powerful tunable electromagnetic Stokes mode might be produced utilising the linked mode technique as a signal wave at the expense of the pump wave.

Several research groups have demonstrated optical parametric oscillation in III-V semiconductor crystals that is brought on by optically generated coherent collective modes so far [22–24]. According to the literature that is currently available, no theoretical framework has yet been created to explore optical parametric amplification in magnetised doped Semiconductor magneto-plasmas like InSb, GaAs, GaSb, InAs, etc. with optical phonons serving as the idler wave. Since these crystal types are frequently partly ionic, optical phonon scattering processes predominate over piezoelectric scattering [25, 26]. In order to understand the basic characteristics of crystals, it is crucial to analyse the coherent optical phonons' propagation characteristics. Due to its enormous potential for the creation of optoelectronic devices, the study of laser-longitudinal optical phonon interactions in Semiconductor magneto-plasmas is currently one of the most active areas of research.

In this paper, attention is focused on analytical investigations of optical parametric oscillation of optical phonon mode in magnetised doped Semiconductor magneto-plasmas using hydrodynamic model of (one component) semiconductor plasma and adopting the coupled mode approach. This is done keeping in mind the potential impact of parametric interactions.

2. Theoretical model

An OPO, in its simplest form, consists of a nonlinear crystal (here III-V semiconductor crystal) placed within an optical resonator and illuminated by an intense laser (pump) beam at ω_0. The pump field gives rise an idler wave at optical phonon frequency ω_{op} and a signal wave at Stokes frequency ω_s. The generated fields at ω_{op} and ω_s get amplified as they travel through the nonlinear crystal. The amplification at ω_{op} and ω_s occurs via parametric interaction among three optical fields viz. pump field, idler field and signal field within the nonlinear crystal. This interaction is a result of nonlinear polarization exhibited by the crystal, which is noncentrosymmetric in nature. For a noncentrosymmetric III-V semiconductor crystal of length *L*, we will determine some operational characteristics such as threshold characteristics and conversion efficiency of the proposed OPO.

Parametric interaction processes have been studied by many researchers both classically as well as quantum mechanically. If there are large numbers of photons in the radiation field, it can be well described classically. In the treatment of coupled wave problems, the classical description is found more appropriate since then the decay or amplification of waves depend on relative phases among them, whereas in quantum mechanical description, if the number of quanta is prescribed, the phases will be undetermined as required by uncertainty principle. Thus, here, classical discussion on parametric interaction among pump field, idler field and signal field within the semiconductor crystal is given. We consider the hydrodynamic model of homogeneous semiconductor plasma. This model restricts our analysis to be valid only in the limit $kl << 1$ (k is the wave number and l is the carrier mean free path).

In order to study single resonant parametric oscillation due to excitation of optical phonon mode, the coupled mode scheme is used. We consider the propagation of a pump wave

$$\vec{E}_0 = \hat{x}E_0 \exp[i(k_0 x - \omega_0 t)] \tag{1}$$

in a III-V semiconductor crystal placed in magnetostatic field $\vec{B}_0 = \hat{z}B_0$; normal to the propagation vectors $\vec{k}_0$, $\vec{k}_{op}$ and $\vec{k}_s$ (all parallel to the *x*-axis) of three interacting waves, viz, pump ($\omega_0, \vec{k}_0$), idler ($\omega_{op}, \vec{k}_{op}$) and signal ($\omega_s, \vec{k}_s$) respectively. The momentum and energy exchange between these waves can be described by phase-matching conditions: $\hbar\vec{k}_0 = \hbar\vec{k}_{op} + \hbar\vec{k}_s$ and $\hbar\omega_0 = \hbar\omega_{op} + \hbar\omega_s$; known as momentum and energy conservation relations, respectively. This yield $\omega_s = \omega_0 - \omega_{op}$ and $\vec{k}_{op} = 2\vec{k}_s = \vec{k}$ (since $|\vec{k}_0| \cong |\vec{k}_s|$). The Stokes mode ($\omega_s, \vec{k}_s$) arises due to coupling of the pump field with density perturbations at an optical phonon frequency ω_{op} in the crystal. The coupling of the pump Stokes field generates a strong electrostatic (space-charge) field oscillating at frequency ω_{op}; which possesses both longitudinal as well as transverse components. In the weakly polar semiconductors (viz., GaAs, InSb), the longitudinal optical (LO) phonons are associated with longitudinal electric field while transverse optical (TO) phonons are accomplished by transverse electrostatic field. The intensities of LO and TO phonons scattering become unrelated for finite $\vec{k}$ because they are determined by two independent parameters, viz., the electro-optical effect and the deformation potential Raman tensor, respectively [27]. The polarization associated with the longitudinal vibration is much larger than the transverse component in III-V crystals like InSb, GaAs, etc. with zinc-blend structures [28]. Consequently, we neglect the transverse electric field and treat ω_{op} as the longitudinal optical phonon frequency.

We consider the weakly polar III-V semiconductor crystal consisting of the two atoms in the molecule vibrating in opposite directions. This diatomic molecule is characterized by its position and normal vibration coordinates $u_{\pm}(x,t)$. In the presence of pump wave, the equation of motion for a single oscillator under one dimensional (1-d) configuration is given by [29, 30]

$$\frac{\partial^2 s}{\partial t^2}+\omega_{opo}^2 s+2\Gamma_{op}\frac{\partial s}{\partial t}=\frac{q_s}{M}E_{op} \tag{2a}$$

where $s(=u_+ + u_-)$ is the relative displacements of positive and negative ions, respectively. E_{op} is the macroscopic internal electrostatic field oscillating at ω_{op}. In equation (2a), ω_{opo} is the optical phonon frequency at $\left|\vec{k}_{op}\right|=0$. Γ_{op} is introduced phenomenologically as a constant parameter and it takes into account the phonon decay. We consider $\Gamma_{op}\approx 10^{-2}\omega_{opo}$ [31-33]. q_s is the Szigeti effective charge [34]. It is convenient to write the relative displacement in terms of new parameter w defined as [35]: $w=(NM)^{1/2}s$. Accordingly, equation (2a) can be expressed as:

$$\frac{\partial^2 w}{\partial t^2}+\omega_{opo}^2 w+2\Gamma_{op}\frac{\partial w}{\partial t}=\left(\frac{q}{M}\right)^{1/2}q_s E_{op}. \tag{2b}$$

Since, the ions in the diatomic molecule possess opposite charges; therefore there will be a net dipole moment in the crystal and hence it induces a polarization ($P=q_s w$). The induced longitudinal phonon electrostatic field (E_{op}), arising due to the induced polarization can be determined from Poission's equation. Consequently, we may express E_{op} in terms of the polarization as:

$$\frac{\partial E_{op}}{\partial x}=-\frac{n_{op}e}{\varepsilon}-\frac{Nq_s}{\varepsilon}\left(\frac{\partial w}{\partial x}\right), \tag{3}$$

where $\varepsilon=\varepsilon_0\varepsilon_\infty$, n_{op} is the perturbed carrier density oscillating at ω_{op} and $-e$ is electronic charge. At the entrance window $x=0$, we consider that the density perturbation n_{op} is negligibly small such that the term $n_{op}(e/\varepsilon)$ in equation (3) may be neglected safely. We obtain

$$E_{op}=\left|\frac{Nq_s}{k\varepsilon}\left(\frac{\partial w}{\partial x}\right)\right|, \tag{4}$$

where we have taken $\left|\vec{k}_{op}\right|=k$ (say). Using equation (2b), the value of E_{op} can be estimated approximately in the weakly polar III-V semiconductor crystals from the knowledge of strain $(\partial w/\partial x)$ [36, 37]. Assuming $(\partial w/\partial x)=10^6$, we get $E_{op}(0)=2.15\times10^5\ \mathrm{Vm^{-1}}$ in n-InSb crystal with $M=2.7\times10^{29}\ \mathrm{kg}$, $N=(a_l^3)=3.7\times10^{27}\ \mathrm{m^{-3}}$, $q_s=1.2\times10^{-20}$, $k=1.86\times10^6\ \mathrm{m^{-1}}$, $\varepsilon_s=17.54$ and $\varepsilon_\infty=15.68$.

The other basic equations considered in the formulation of $\chi^{(2)}$ are:

$$\frac{\partial n_1}{\partial t}+v_0\frac{\partial n_1}{\partial x}+n_1\frac{\partial v_0}{\partial x}+n_0\frac{\partial v_1}{\partial x}=0 \tag{5}$$

$$\frac{\partial \vec{v}_0}{\partial t}+\nu\vec{v}_0+\left(\vec{v}_0.\frac{\partial}{\partial x}\right)\vec{v}_0=-\frac{e}{m}[\vec{E}_0+(\vec{v}_0\times\vec{B}_0)]=-\frac{e}{m}(\vec{E}_{eff}) \tag{6}$$

$$\frac{\partial \vec{v}_1}{\partial t}+\nu\vec{v}_1+\left(\vec{v}_0.\frac{\partial}{\partial x}\right)\vec{v}_1+\left(\vec{v}_1.\frac{\partial}{\partial x}\right)\vec{v}_0=\frac{e}{m}[\vec{E}_1+(\vec{v}_1\times\vec{B}_0)]. \tag{7}$$

These equations and the symbols used have been well described in Ref. [22, 23]. In order to obtain the coupled mode equation for the optical phonon flux, we consider the density perturbations to vary as: $n_{op}\propto\exp[i(k_{op}x-\omega_{op}t)]$ and $n_s\propto\exp[i(k_s x-\omega_s t)]$. Using equation (5), these density perturbations can be obtained as:

$$n_{op}=\frac{k}{\omega_{op}}(n_s v_0+n_0 v_{op}) \tag{8a}$$

and

$$n_s=\frac{k}{\omega_s}(n_{op}v_0^*+n_0 v_s). \tag{8b}$$

Here, $v_{op}=-\frac{e}{m}\frac{(\nu-i\omega_{op})E_{op}}{[\omega_c^2+(\nu-i\omega_{op})^2]}$

and $v_s=-\frac{e}{m}\frac{(\nu-i\omega_s)E_s}{[\omega_c^2+(\nu-i\omega_s)^2]}$,

with $n_1=n_{op}+n_s$ and $v_1=v_{op}+v_s$.

$\omega_c=(e/m)B_0$ is the electron-cyclotron frequency. Substitution of values of u and n_{op} from equations (2a) and (8a) respectively, in equation (3) and simple mathematical simplification yield

$$\left(1+\frac{Nq_s^2}{\varepsilon M\omega_{pp}^2}\right)\frac{\partial E_{op}}{\partial x}=\frac{ek}{\varepsilon\omega_{op}}(n_s v_0+n_0 v_{op}), \tag{9}$$

where $\omega_{pp}^2=\omega_{opo}^2-\omega_{op}^2-2i\Gamma_{op}\omega_{op}$.

Equation (9) reveals that the coupling of the perturbed electron density and oscillatory electron fluid velocity act as a disturbed source that can feed energy to the induced optical phonon field (E_{op}) leading to the amplification of this field with a large gain coefficient. We may express equation (9) in terms of the coupled electric fields. Using equations (4) – (6) and (9), the induced longitudinal optical phonon flux can be expressed as:

$$\frac{\partial E_{op}}{\partial x}+\alpha_{op}E_{op}=i\beta_{op}E_0(x)E_s(x). \tag{10a}$$

Here $\alpha_{op}E_{op}$ is introduced phenomenologically to take into account the absorption processes in the crystal; α_{op} being the absorption coefficient in the off-resonant regime. β_{op} may be treated as the coupling parameter which can be obtained from the above formulations as:

$$\beta_{op}=\frac{-iek^2\omega_0}{m\omega_{op}(\omega_0^2-\omega_c^2)}\left[1+\frac{Nq_s^2}{\varepsilon M\omega_{pp}^2}+\frac{i\omega_p^2(\nu-i\omega_{op})}{\omega_{op}[(\nu-i\omega_{op})^2+\omega_c^2]}\right]^{-1} \tag{10b}$$

In deriving equation (10b), we assumed $\omega_0, \omega_s \gg \nu$.

The induced nonlinear polarization P_{NL} arising due to the nonlinear current density given by

$$\vec{P}_{NL} = \int \vec{J} dt = \int (\vec{J}_1 + \vec{J}_2) dt = -\int (n_0 e v_s + n_{op} e v_0^*) dt \,, \tag{11}$$

where $\vec{J} = \vec{J}_0 + \vec{J}_1$ represents the total induced current density in the crystal and it comprises of zeroth-order ($\vec{J}_0$) as well as perturbed components oscillating at the Stokes frequency $\vec{J}_1$.

The complex optical susceptibility $\chi = \chi_r + i\chi_i$ can be obtained from:

$$P_{NL} = \varepsilon_0 \chi E = \varepsilon_0 [\chi^{(1)} + \chi^{(2)} E] E \tag{12}$$

In equation (12), we have truncated the expression up to the second-order nonlinear optical susceptibility ($\chi^{(2)}$) since the origin of the three-wave parametric interactions lies in $\chi^{(2)}$ of the medium. Following the method adopted in Ref. [22] and using equations (2b) - (6), (11) and (12), we obtain

$$\chi_i^{(1)} = \frac{\varepsilon_\infty \nu \omega_p^2 \delta_s}{\omega_s^3 [\delta_s^2 + (\nu^2 / \omega_s^2)]} \tag{13}$$

and

$$\chi^{(2)} = \frac{-iekNq_s^2 \omega_p^2}{\varepsilon_0 mM \omega_0 \omega_s \delta_0 \delta_s \omega_{pp}^2 \Omega^2} \,, \tag{14}$$

where $\delta_0 = 1 - \frac{\omega_c^2}{\omega_0^2}$, $\delta_s = 1 - \frac{\omega_c^2}{\omega_s^2}$ and

$\Omega^2 = \frac{\omega_p^2}{\delta_s} - \omega_{op}^2 + i\nu\omega_{op}$, in which

$\omega_p = \left(\frac{n_0 e^2}{m\varepsilon} \right)^{1/2}$ is the electron-plasma frequency.

Using the slowly varying envelope approximation (SVEA) [38], let us now obtain an expression for threshold pump intensity of SRPO including the attenuation losses caused by mirror transmission as well as absorption and scattering inside the cavity. In order to obtain the steady state coupled mode equations for the pump and the Stokes waves, we employ Maxwell's equations in the presence of a finite induced nonlinear polarization P_{NL} arising due to the nonlinear current density given by

$$\nabla^2 \vec{E} = \frac{1}{c^2} \frac{\partial^2 \vec{E}}{\partial t^2} - \mu_0 \frac{\partial^2 \vec{P}_{NL}}{\partial t^2} \,. \tag{15}$$

where c is the velocity of light in the crystal.

Using equations (11) and (15) and employing SVEA, the equations describing the collinear OPO fields can be represented in terms of complex amplitudes as:

$$\frac{\partial E_0}{\partial x} + \alpha_0 E_0 = i\beta_0 E_{op} E_s^* \tag{16a}$$

and

$$\frac{\partial E_s}{\partial x} + \alpha_s E_s = i\beta_s E_{op} E_0^* \,. \tag{16b}$$

Equations (16a) and (16b) represent the coupling between the pump and the backward scattered Stokes wave via the optical phonon mode in the medium. α_0 and α_s are the inherent backward absorption coefficients corresponding to pump wave frequency (ω_0) and Stokes wave frequency (ω_s), respectively. These are defined as:

$$\alpha_0 = \left(\frac{\omega_0}{\eta c} \right) \chi_i^{(1)} \tag{17a}$$

and

$$\alpha_s = \frac{\omega_s}{\eta c} \chi_i^{(1)} \,, \tag{17b}$$

where $\chi_i^{(1)}$ is the imaginary part of linear optical susceptibility [Eq. (13)] and η is the crystal background refractive index.

Moreover $k_0 = \frac{\eta\omega_0}{c}$ and $k_s = \frac{\eta\omega_s}{c}$.

In equations (16a) and (16b), β_0 and β_s are the coupling parameter defined as:

$$\beta_0 = \left(\frac{\omega_0}{\eta c} \right) \chi^{(2)} \tag{18a}$$

and

$$\beta_s = \left(\frac{\omega_s}{\eta c} \right) \chi^{(2)} \,, \tag{18b}$$

where $\chi^{(2)}$ is the second-order optical susceptibility [Eq. (14)] of semiconductor crystal in the presence of magnetostatic field.

We now address ourselves to the analytical study of threshold pump intensity and operational characteristics of SRPO. We employ equations (10a) and (16b) and solve them assumed solution of the forms

$$E_{op}(x) = C_1 \exp(\gamma x) \tag{19a}$$

and

$$E_s(x) = C_2 \exp(\gamma x) \,, \tag{19b}$$

where C_1 and C_2 are the arbitrary constants and γ is the gain coefficient. One may recall that the parametric interactions yield identical gain coefficients for both the idler and signal waves. The gain coefficient can be determined by

using equations (10a) and (16b) through equations (19a) and (19b). Simplification yield

$$\gamma_0 = \left(\alpha_-^2 - \frac{8\beta_{op}\beta_{o,s} I_0}{\eta\varepsilon_0 c} \right)^{1/2}. \quad (20)$$

We obtain

$$\gamma_\pm = \frac{-\alpha_s \pm \gamma_0}{2}, \quad (21)$$

where $\gamma_0 = \left(\alpha_-^2 - \frac{8\beta_{op}\beta_{os} I_0}{\eta\varepsilon_0 c} \right)^{1/2}$,

in which $I_0 = (1/2)\eta\varepsilon_0 c|E_0|^2$ is the pump field intensity. For simplicity, we consider $\alpha_\pm = \alpha_{op} + \alpha_s$. Also we have assumed $\beta_0 = \beta_s = \beta_{0s}$ for $\omega_0 \sim \omega_s \gg \omega_{op}$.

Consequently, form equations (19a) and (19b), we get

$$E_{op}(x) = \exp\left(-\frac{\alpha_+ x}{2}\right)\left[C_{1+} \exp\left(\frac{\gamma_0 x}{2}\right) + C_{1-} \exp\left(\frac{-\gamma_0 x}{2}\right) \right] \quad (22a)$$

and

$$E_s(x) = \exp\left(-\frac{\alpha_+ x}{2}\right)\left[C_{2+} \exp\left(\frac{\gamma_0 x}{2}\right) + C_{2-} \exp\left(\frac{-\gamma_0 x}{2}\right) \right]. \quad (22b)$$

In order to study the parametric oscillations in the weakly polar semiconductor crystal, let us consider $E_{op}(0)$ and $E_s(0)$ to be finite due to finiteness of lattice vibrations and spontaneous noise field, respectively. These considerations enable one to determine the signal and the idler fields at the exit window $x = L$ with L being the sample length. Using the above boundary conditions, we obtain

$$C_{1+} = \frac{1}{2\gamma_0}\left[(\gamma_0 \mp \alpha_-) E_{op}(0) \pm 2i\beta_{op} E_0(0) E_s(0) \right] \quad (23a)$$

and

$$C_{2+} = \frac{1}{2\gamma_0}\left[(\gamma_0 \pm \alpha_-) E_s(0) \pm 2i\beta_{0s} E_{op}(0) E_0^*(0) \right]. \quad (23b)$$

We also obtain

$$E_{op}(L) = \exp\left(\frac{-\alpha_+ L}{2}\right)\left[\left\{ \cosh(\gamma_0 L) - \left(\frac{\alpha_-}{\gamma_0}\right)\sinh(\gamma_0 L) \right\} E_{op}(0) + \left(\frac{2i\beta_{op}}{\gamma_0}\right) E_0(0) E_s(0) \sinh(\gamma_0 L) \right] \quad (24a)$$

and

$$E_s(L) = \exp\left(\frac{-\alpha_+ L}{2}\right)\left[\left\{ \cosh(\gamma_0 L) - \left(\frac{\alpha_-}{\gamma_0}\right)\sinh(\gamma_0 L) \right\} E_s(0) + \left(\frac{2i\beta_{op}}{\gamma_0}\right) E_{op}(0) E_0^*(0) \sinh(\gamma_0 L) \right]. \quad (24b)$$

Equations (24a) and (24b) describe the output signal and idler waves $x = L$ (i.e. end of the crystal of length).

In order to study the threshold pump intensity and the basic operational characteristic of OPO, we consider that the crystal satisfying equations (24a) and (24b) is kept inside an optical cavity such that we can have feedback of Stokes field. If the parametric amplified power gain is sufficiently high, a parametric oscillator can be constructed [39]. The consideration of feedback mechanism makes it possible for the parametric gain to overcome the losses and subsequently parametric oscillations occur.

In the present chapter, we have made an attempt to establish the weakly polar III-V semiconductor crystals as the class of materials suitable for the development of SRPO. The SRPO has many advantages over the double resonant parametric oscillator (DRPO) except that it requires large threshold pump intensity. Therefore, we have chosen SRPO for the present study. The optical cavity configuration for SRPO has been chosen such that the second mirror located at exit window of the cavity is strongly reflective at the Stokes wave frequency ω_s whereas, for the pump and optical phonon frequencies ω_0 and ω_{op}, both the mirrors are nearly transparent. We have taken R_s as the Stokes field reflectivity parameter of the second mirror. In this analysis, we have neglected the phase shifts in phonon and Stokes field due to traversal and reflection in the cavity [40]. For simplicity it is also assumed that the cavity length is equal to the crystal length L. In order to reduce the threshold value of the pump intensity and to enhance the power gain of the optical phonon modes well above the threshold, we have employed the round-trip mechanism. Under such circumstances, the threshold condition can be given by

$$R_s |E_s(L)| = |E_s(0)|. \quad (25)$$

Physically, equation (25) illustrates that the Stokes field undergoes neither amplification nor attenuation during one round-trip. While considering the attenuation loss due to absorption and scattering in the cavity as well as the mirror transmission loss, the total loss in the cavity may be expressed as [41]:

$$\alpha_{T+} = \alpha_\pm - \frac{1}{L}(\ln R_s). \quad (26)$$

Using Eqs. (24b), (25) and (26), we obtain

$$\left| \exp\left(\frac{-\alpha_{T+} L}{2}\right) \mathrm{Re}(\beta_{0s}) R_s E_{op}(0) \sinh(\gamma_0' L) \right| = \left| \gamma_0' \frac{E_s(0)}{E_0(0)} \right|, \quad (27)$$

where $\gamma_0' = \left[4\alpha_{T-}^2 + \left(\frac{8I_0\,\mathrm{Re}(\beta_{op}\beta_{0s})}{\eta\varepsilon_0 c}\right)\right]^{1/2}$; $E_s(0) \ll E_0(0)$.

The threshold pump intensity for SRPO can be obtained by differentiating equation (27) with respect to γ_0' as:

$$I_{0th} = \left|\frac{\eta\varepsilon_0 c}{8\,\mathrm{Re}(\beta_{op}\beta_{0s})}\left[\frac{1}{L^2}\left\{\cosh^{-1}\left(\frac{1}{Q}\right)\right\}^2 - 4\alpha_{T-}^2\right]\right|, \qquad (28)$$

where $Q = \frac{E_0(0)}{E_s(0)}\left[LR_s E_{op}(0)\,\mathrm{Re}(\beta_{0s})\exp\left(\frac{-\alpha_{T+}L}{2}\right)\right]$.

The conversion efficiency η_k is defined as the ratio of the idler (signal) output energy to the incident pump energy. In order to estimate the conversion efficiency of the parametric oscillator, relation between the idler (signal) power to constant signal (idler) power must be known. In the present article, this relation can be derived from the set of coupled mode equations (10) and (16a). In doing so, we have assumed the signal field (Stokes mode) as constant during single round-trip. Solving equations (10) and (16a) and obtained simplified solution of the idler mode as:

$$E_{op}(L) = \exp(-\alpha_{T+}L)\left[\left\{\cosh(\gamma_2 L) - \left(\frac{\alpha_{T-}}{\gamma_1}\right)\sinh(\gamma_2 L)\right\}E_{op}(0) + \left(\frac{2i\beta_{op}}{\gamma_1}\right)E_0(0)E_s(0)\sinh(\gamma_2 L)\right], \qquad (29)$$

where $\gamma_1 = -\alpha_{T-} + \gamma_2$, $\gamma_2 = \left[\alpha_{T-}^2 + \mathrm{Re}(\beta_{op}\beta_{0s})|E_s|^2\right]^{1/2}$.

Using equation (29) and the definition of η_k as given above, we can have

$$\eta_k = \frac{|E_{op}(L)|^2}{|E_0(0)|^2}. \qquad (30)$$

Equation (30) may be used to determine the conversion efficiency of the proposed SRPO, respectively.

3. Results and discussion

In this section, we address the detailed numerical analysis of the threshold and operational characteristics of SRPO consisting of magnetized doped III-V semiconductor crystals. The following set of material parameters has been used to perform numerical appreciation of the results obtained and the crystal is assumed to be irradiated by 10.6 μm CO_2 laser [24, 31]:

$m = 0.015m_0$, $\rho = 5.8\times10^3$ kg m^{-3}, $\varepsilon_L = 17.8$, $\varepsilon_\infty = 15.68$, $\nu = 3.5\times10^{11}$ s^{-1}, $\omega_{op} = 3.7\times10^{13}$ s^{-1}, $n_0 = 10^{19} - 10^{24}$ m^{-3}, $M = 2.7\times10^{-29}$ kg, $N = 1.48\times10^{28}$ m^{-3}, $q_s = 1.2\times10^{-20}$ C, $\alpha_u = 1.68\times10^{-16}$ SI units.

This set of data is related to a typical n-InSb crystal, however, the results obtained in previous section may be applied to any III-V semiconductor crystal.

The nature of dependence of the threshold pump intensity $I_{0,th}$ of SRPO on different parameters such as externally applied magnetostatic field B_0, mirror reflectivity R, crystal length L etc. may be studied from equation (28). The results are plotted in Figs. 1 – 3.

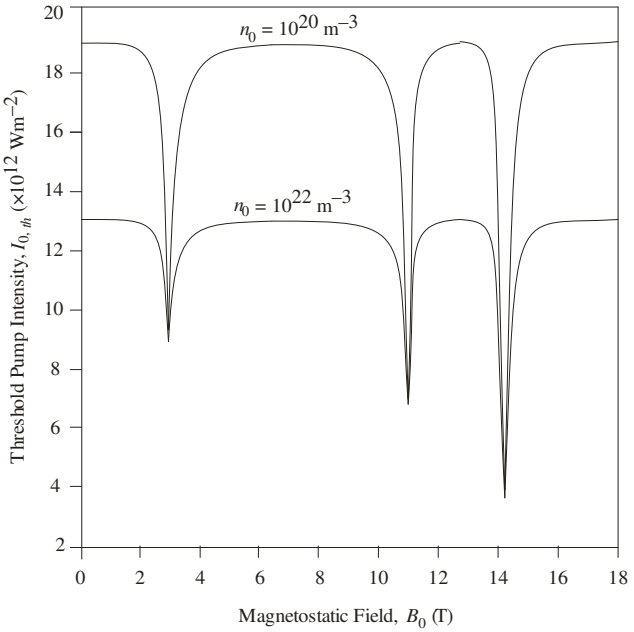

Figure 1. Variation of threshold pump intensity $I_{0,th}$ of SRPO with magnetostatic field B_0 with $R = 95\%$, $L = 0.3$ mm for two different doping concentrations n_0.

Figure 1 shows the variation of threshold pump intensity $I_{0,th}$ of SRPO with magnetostatic field B_0 with $R = 95\%$, $L = 0.3$ mm for two different values of doping concentration (n_0 = 10^{20}m^{-3} and $n_0 = 10^{22}$m^{-3}). It can be observed that in both the cases, $I_{0,th}$ starts with a high value in the absence of B_0; remains nearly constant for $B_0 \le 2$ T and decreases sharply attaining a minimum value ($I_{0,th} = 9\times10^{12}$ Wm^{-2}) at $B_0 = 3$ T. With increasing B_0 beyond this value, $I_{0,th}$ increases sharply and remains constant over a wide range of B_0 ($\approx 4-10$ T). With further increasing B_0, $I_{0,th}$ again decreases sharply attaining a minimum value at $B_0 = 11$ T. With further increasing B_0 beyond this value, $I_{0,th}$ increases sharply and again remains constant over a narrow range of B_0 ($\approx 12-13$ T). With further increasing B_0 beyond this value, $I_{0,th}$ again decreases sharply attaining a minimum value at $B_0 = 14.2$ T. Beyond this value of B_0, $I_{0,th}$ again increases sharply and becomes independent of magnetostatic field. The dip at $B_0 = 3$T, 11T and 14.2T may be attributed to resonance conditions: $\omega_c^2 \sim \omega_{op}^2$, $\omega_c^2 \sim \omega_s^2$ and $\omega_c^2 \sim \omega_0^2$ respectively. A comparison between two cases reveals that except at resonance conditions:

$$(I_{0,th})_{n_0=10^{22}\,\mathrm{m}^{-3}} < (I_{0,th})_{n_0=10^{20}\,\mathrm{m}^{-3}}.$$

At resonance conditions, $I_{0,th}$ becomes independent of n_0. Hence, an external magnetostatic field plays an important role

in reducing the threshold pump intensity of SRPO in Semiconductor magneto-plasmas around resonance conditions.

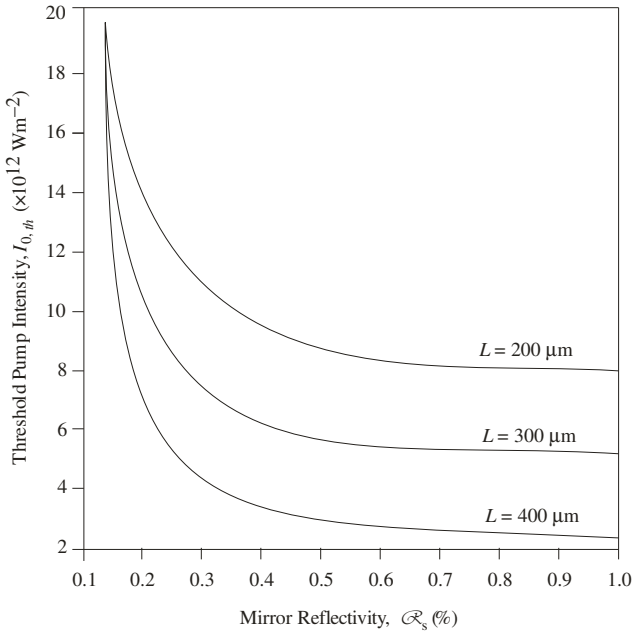

Figure 2. Variation of threshold pump intensity $I_{0,th}$ of SRPO with mirror reflectivity R with B_0 = 14.2T (because at this particular value of B_0, $I_{0,th}$ is minimum), $n_0 = 10^{22}$m^{-3} for three different values of crystal length L.

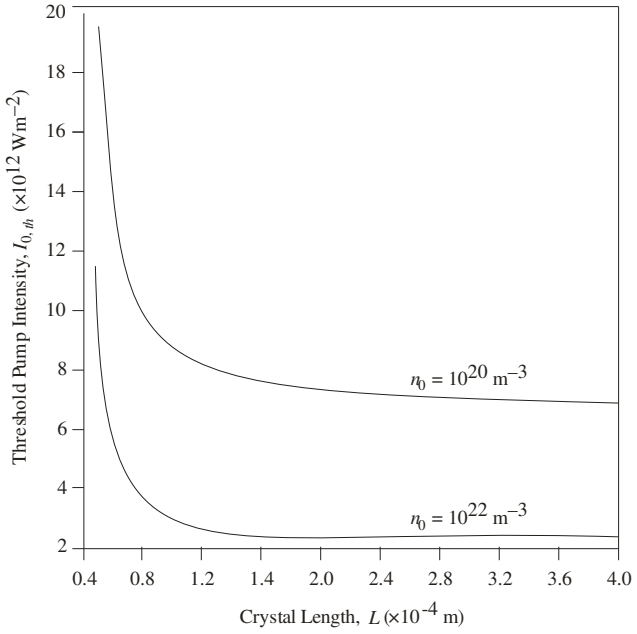

Figure 3. Variation of threshold pump intensity $I_{0,th}$ of SRPO with crystal length L with mirror reflectivity R = 95%, B_0 = 14.2T for two different values of doping concentration n_0.

Figure 2 shows the variation of threshold pump intensity $I_{0,th}$ of SRPO with mirror reflectivity R with B_0 = 14.2T (because at this particular value of B_0, $I_{0,th}$ is lowest) and $n_0 = 10^{22}$m^{-3} for three different values of crystal length L. It can be observed that for R = 15%, $I_{0,th}$ is very high, independent of L and all the curves coincide. With increasing mirror reflectivity, $I_{0,th}$ decreases very rapidly for R < 40%; the increase in mirror reflectivity increases the net gain per round trip at the signal wavelength resulting in lower oscillation threshold intensity for high reflectivity. For R > 40%, the rate of fall of threshold intensity is very small. Moreover, with increasing crystal length, the rate of threshold intensity is faster. Hence, we conclude from this figure that threshold pump intensity of SRPO in Semiconductor magneto-plasmas can be effectively reduced by increasing the crystal length and mirror reflectivity $R \sim 40\%$.

Figure 3 shows the variation of threshold pump intensity $I_{0,th}$ of SRPO with crystal length L with mirror reflectivity R = 95% and B_0 = 14.2T for two different values of doping concentration n_0. It can be observed that for a given doping concentration, $I_{0,th}$ is very large for $L = 50\mu m$ and decreases quite sharply for $50\mu m < L < 120\mu m$. Beyond this value of crystal length, $I_{0,th}$ becomes nearly independent of L. Moreover, the highly doped semiconductor crystal yields lower of threshold pump intensity for same crystal length.

Hence we conclude from figures 2 and 3 that threshold pump intensity of SRPO can be lowered by increasing crystal (or cavity) length, mirror reflectivity and doping concentration.

Using the material parameters (for n-Insb) given above, the nature of dependence of conversion efficiency on different parameters such as externally applied magnetostatic field B_0, doping concentration n_0, pump field intensity I_0, crystal length etc. well above the threshold pump intensity may be studied from equations (30) and (31), respectively. The results are plotted in Figs. 4 – 9.

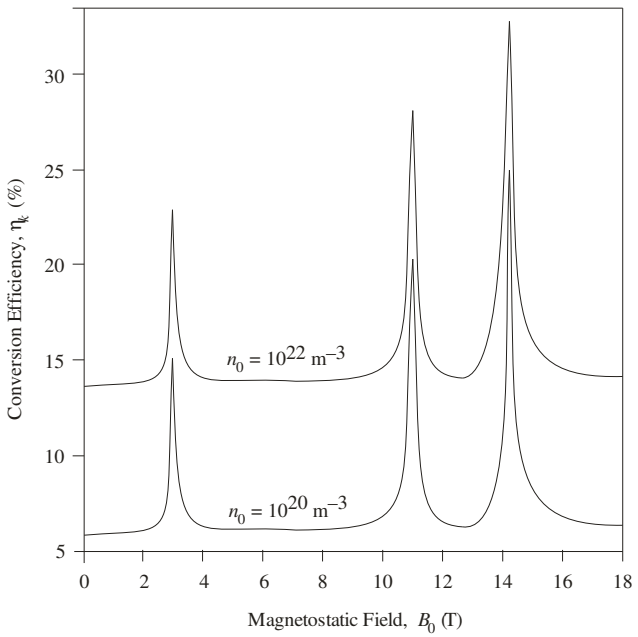

Figure 4. Nature of dependence of conversion efficiency η_k on externally applied magnetostatic field B_0 with R = 95%, L = 0.3 mm and $I_0 = 6.5\times10^{13}$ Wm^{-2} for two different values of doping concentration n_0.

Figure 4 shows the nature of dependence of conversion efficiency η_k on externally applied magnetostatic field B_0 with R = 95%, L = 0.3 mm and $I_0 = 6.5\times10^{13}$ Wm^{-2} for two different values of doping concentration n_0. In both the cases, η_k is nearly independent of B_0 except at 3 T, 11 T and 14.2 T. At these particular values of B_0, η_k shows sharp peaks due to

resonance conditions ($\omega_c^2 \sim \omega_{op}^2, \omega_c^2 \sim \omega_s^2$ and $\omega_c^2 \sim \omega_0^2$ respectively). On comparing the three peaks, we note that

$$(\eta_k)_{B_0=14.2\text{T}} : (\eta_k)_{B_0=11\text{T}} : (\eta_k)_{B_0=3\text{T}} = 1.43 : 1.17 : 1 .$$

Moreover, we observed that with increasing n_0 from 10^{20}m^{-3} to 10^{22}m^{-3}, η_k becomes almost 1.5 times. Hence, we conclude from this figure that conversion efficiency of SRPO can be enhanced by proper selection of magnetostatic field (around resonance conditions: $\omega_c^2 \sim \omega_{op}^2, \omega_c^2 \sim \omega_s^2$ and $\omega_c^2 \sim \omega_0^2$) and increasing doping concentration.

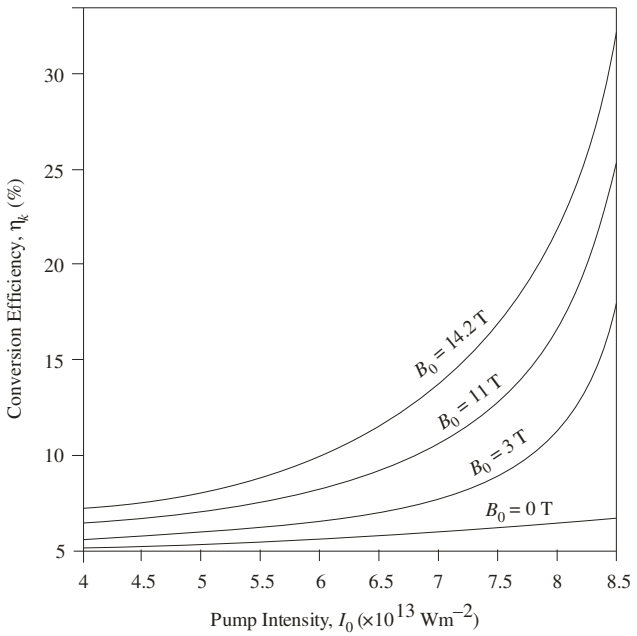

Figure 5. Nature of dependence of conversion efficiency η_k on pump intensity I_0 for: (i) absence of magnetostatic field (B_0 = 0T), and (ii) presence of magnetostatic field (B_0 =3 T, 11 T, 14.2 T).

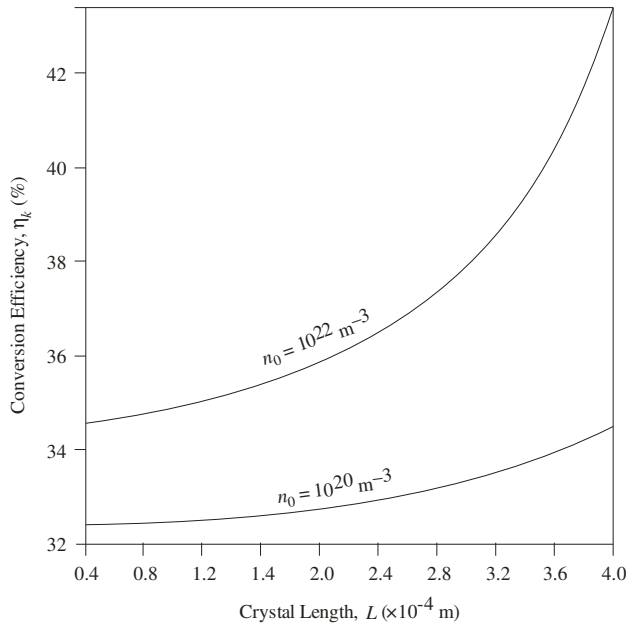

Figure 6. Nature of dependence of conversion efficiency η_k on crystal length L with R = 95%, B_0 = 14.2T and $I_0 = 6.5\times10^{13}$ Wm^{-2} for two different values of doping concentration n_0.

Figure 5 shows the nature of dependence of conversion efficiency η_k on pump intensity I_0 with R = 95%, L = 0.3 mm and n_0 = 10^{22}m^{-3} for different cases, viz. (i) absence of magnetostatic field (B_0 = 0T), and (ii) presence of magnetostatic field (B_0 = 3 T, 11 T, 14.2 T). We observed that in the absence of magnetostatic field, η_k is very small and increases linearly with I_0. In the presence of magnetostatic field, η_k increases linearly with I_0 ($\leq 7\times10^{13}$ Wm^{-2}). Beyond this point, η_k increases quadrically with I_0. Such a behavior agrees well with the theoretically calculated values [42, 43] and experimental observations [44, 45]. Moreover, $(\eta_k)_{B_0=14.2\text{T}} > (\eta_k)_{B_0=11\text{T}} > (\eta_k)_{B_0=3\text{T}}$ and the effect of magnetostatic field is more pronounced at higher pump intensities. We obtained $\eta_k = 33\%$ at B_0 = 14.2T, which is limited by available pump power rather than crystal damage or intra-cavity losses. Hence we conclude from this figure that conversion efficiency of SRPO can be enhanced by increasing the pump intensity and externally applied magnetostatic field; the effect of magnetostatic field is more pronounced at high pump intensities.

Fig. 6 shows the nature of dependence of conversion efficiency η_k on crystal length L with R = 95%, B_0 = 14.2T and $I_0 = 6.5\times10^{13}$ Wm^{-2} for two different values of doping concentration n_0. We observed that in both the cases η_k increases quadrically with L. The growth rate of η_k in case of heavy doping is more. Hence, it is clear that the effect of doping concentration is more pronounced for larger crystal lengths.

4. Conclusions

In the present study, a detailed numerical analysis of the threshold and operational characteristics of SRPO consisting of magnetized doped III-V semiconductor crystals have been undertaken. The hydrodynamic model of semiconductor-plasma has been successfully applied to study the influence of different parameters such as externally applied magnetostatic field, doping concentration, mirror reflectivity, crystal length etc. on threshold pump intensity and conversion efficiency of SRPO consisting of III-V semiconductor crystal duly irradiated by slightly off-resonant laser pulsed laser. An externally applied magnetostatic field plays an important role in reducing the threshold pump intensity of SRPO in Semiconductor magneto-plasmas around resonance conditions. The threshold pump intensity of SRPO can be lowered by increasing crystal (or cavity) length, mirror reflectivity and doping concentration. The conversion efficiency of SRPO can be enhanced by proper selection of magnetostatic field (around resonance conditions) and increasing doping concentration. The technological potentiality of transversely magnetized doped III-V semiconductor crystals as the hosts for parametric devices like parametric oscillators has been established.

References

[1] R.L. Sutherland, Handbook of Nonlinear Optics, Marcel Dekker, New York (2003).
[2] R.W. Boyd, Nonlinear Optics, Academic Press, New York (2008).
[3] K. Rottwitt, P.T. Lichtenberg, Nonlinear Optics: Principles and Applications, CRC Press, New York (2014).

[4] G.P. Agarwal, Applications of Nonlinear Fiber Optics, Academic Press, New York (2001).
[5] E. Garmire, Nonlinear optics in daily life, *Opt. Exp*. **21** (2013) 30532 – 30544.
[6] C.K. Hong, L. Mandel, Theory of parametric frequency down conversion of light, *Phys. Rev. A* **31** (1985) 2409-2418.
[7] Z.Y. Ou, L.J. Wang, L. Mandel, Photon amplification by parametric down conversion, *J. Opt. Soc. Am. B* **7** (1990) 211-214.
[8] R.L. Bayer, Nonlinear Optics, Academic Press, London (1975).
[9] A.G. Ciriolo , M. Negro , M. Devetta, E. Cinquanta, D. Faccialà, A. Pusala, S.D. Silvestri, S. Stagira, C. Vozzi, Optical parametric amplification techniques for the generation of high-energy few-optical-cycles IR pulses for strong field applications, *Appl. Sci*. **7** (2017) 265.
[10] A.E. Martin, G.K. Samanta, K. Devi, S.C. Kumar, M.E. Zadeh, Frequency-modulation-mode-locked optical parametric oscillator, *Opt. Lett*. 37 (2012) 115-117.
[11] V. Ulvila, C.R. Phillips, L. Halonen, M. Vainio, Optical frequency comb generation by continuous-wave pumped optical parametric oscillator based on cascading $\chi^{(2)}$ nonlinearities, *Opt. Lett*. **38** (2013) 4281-4284.
[12] R.C. Bapna, C.S. Rao, K. Dasgupta, Low-threshold operation of a 355 – nm pumped nanosecond β-BaB_2O_4 optical parametric oscillator, *Opt. Laser Tech*. **40** (2008) 832-837.
[13] G.K. Samanta, M. Ebrahim-Zadeh, Continuous-wave singly-resonant optical parametric oscillator with resonant wave coupling, *Opt. Exp*. **16** (2008) 6883-6888.
[14] S. Zou, M. Gong, Q. Liu, P. Yan, G. Chen, Gain width and time rise studies of pulsed unstable optical parametric oscillators, *Appl. Phys. B* **81** (2005) 1101-1106.
[15] A.I. Vodchits, V.I. Dashkevich, N.S. Kazak, V.K. Pavlenko, V.I. Pokryshkin, I.P. Petrovich, V.V. Rukhovets, A.S. Kraskovskii, V.A. Orlovich, Eye-safe radiation source based on an optical parametric oscillator, *J. Appl. Spectrosc*. **73** (2006) 285-291.
[16] O.B. Jensen, M. Brunn-Larsen, O. Balle-Petersen, T. Skettrup, Yellow nanosecond sum-frequency generating optical parametric oscillator using periodically poled $LiNbO_3$, *Appl. Phys. B* **91** (2008) 61-63.
[17] B. Ruffng, A. Nebel, R. Wallenstein, High-power picosecond LiB3O5 optical parametric oscillators tunable in the blue spectral range, *Appl. Phys. B* **72** (2001) 137-149.
[18] N.M. Ravindra, P. Ganapathy, J. Chio, Energy-gap refractive index relations in semiconductors – an overview, *Infrared Phys. Technol.* **50** (2007) 21-29.
[19] J. Meyer, M.R. Kruer, F. Bartoli, Optical heating in semiconductors: Laser damage in Ge, Si, InSb, and GaAs, *J. Appl. Phys*. **51** (1980) 5513-5522.
[20] E. Garmire, Resonant optical nonlinearities in semiconductors, *IEEE J. Selected Topics in Quantum Electron*. **6** (2000) 1094-1110.
[21] V. Kumar, A. Sinha, B.P. Singh, S. Chandra, Second-order nonlinear optical susceptibilities of $A^{II}B^{VI}$ and $A^{III}B^{V}$ semiconductors, *Phys. Lett. A* **380** (2016) 3630-3633.
[22] P. Aghamkar, S. Suta, Efficient parametric oscillation in the presence of a magnetic field, *Proc. SPIE*, **4751** (2002) 71-76.
[23] Sandeep, S. Dahiya, N. Singh, Parametric excitation of optical phonons in weakly-polar narrow band gap magnetized semiconductor plasmas, *Mod. Phys. Lett. B* **31** (2017) 1750294.
[24] S. Dubey, S. Ghosh, Parametric oscillations of polaron modes in magnetized semiconductor plasmas, *New J. Phys*. **11** (2009) 093030.
[25] L.A. Falkovsky, Electron-phonon interaction and coupled phonon-plasmon modes, *J. Exp. Theor. Phys*. **97** (2003) 794-805.
[26] A. Hauber, S. Fahy, Scattering of carriers by coupled plasmon-phonon modes in bulk polar semiconductors and polar semiconductor heterostructures, *Phys. Rev. B* **95** (2017) 045210.
[27] M. Cardona, Light Scattering in Solids I, Springer-Verlag, New York (1983).
[28] S.S. Mitra, N.E. Massa, Handbook on Semiconductors, North-Holland, Netherlands (1982).
[29] W. Jones, N.M. March, Theoretical Solid State Physics, Dover (1985).
[30] M. Singh, P. Aghamkar, N. Kishore, P.K. Sen, M.R. Perrone, Stimulated Raman scattering in weakly polar transversely magnetized doped semiconductors, *Phys. Rev. B* **76** (2007) 012302.
[31] M. Singh, Dependence on geometry of coherent Raman scattered Stokes mode in weakly polar magnetized semiconductors, *Physica B*, **403** (2008) 3985-3989.
[32] K. Nishikawa, Parametric excitation of coupled waves I: General formulation, *J. Phys. Soc. Jpn*. **24** (1968) 916-922.
[33] K. Nishikawa, Parametric excitation of coupled waves II: Parametric plasmon-photon interaction, *J. Phys. Soc. Jpn*. **24** (1968) 1152-1158.
[34] J. Callaway, Quantum Theory of the Solid State, Academic Press, New York (1974).
[35] K. Seeger, Semiconductor Physics, Springer Verlag, Berlin (1989).
[36] A. Yariv, P. Yeh, Optical Waves in Crystals, John Wiley, New York (1984).
[37] G.K. Celler, R. Bray, Effect of screening of piezoelectric phonon fields on absorption-edge broadening in GaAs, *Phys. Rev. Lett*. **37** (1976) 1422.
[38] K.D. Shaw, On the slowly varying envelope approximation in coupled-wave theory, *Opt. Commun*. **85** (1991) 191-194.
[39] R. L. Byer, Quantum Electronics, Academic Press, New York (1975).
[40] G. Bjork, Y. Yamamoto, Phase correllation in nondegenerate parametric oscillators and amplifiers: Theory and applications, *Phys. Rev. A* **37** (1988) 1991.
[41] Y.R. Shen, The Principle of Nonlinear Optics, John Wiley, New York (1984).
[42] S.J. Brosnan, R.L. Byer, Optical parametric oscillator threshold and linewidth studies, *IEEE J. Quantum Electron*. **15** (1979) 415-431.
[43] Y.X. Fan, R.C. Eckardt, R.L. Byer, R.K. Route, R.S. Feigelson, $AgGaS_2$ infrared parametric oscillator, *Appl. Phys. Lett*. **45** (1984) 313-315.
[44] R.C. Eckardt, Y.X. Fan, R.L. Byer, Broadly tunable infrared parametric oscillator using $AgGaSe_2$, *Appl. Phys. Lett*. **49** (1986) 608-610.
[45] M. Ebrahimzadeh, M.H. Dunn, F. Akerboom, Highly efficient visible urea optical parametric oscillator pumped by a XeCl excimer laser, *Opt. Lett*. **11** (1989) 560-562.
[1] G.K. Samanta, A. Aadhi, M. Ebrahim-Zadeh, Continuous-wave two-crystal, singly-resonant optical parametric oscillator: theory and experiment, *Opt. Exp*. **21** (2013) 9520-9540.